# Effect of air bubbles in concrete on the mechanical behavior of RC beams strengthened in flexion by externally bonded FRP plates under uniformly distributed loading

Benferhat Rabia[1,2], Tahar Hassaine Daouadji[1,2*] and Rabahi Abderezak[1,2]

*[1]Laboratory of Geomatics and sustainable development, University of Tiaret, Algeria*
*[2]Department of Civil Engineering, Ibn Khaldoun University of Tiaret, Algeria*

**Abstract.** This article presents a theoretical study taking into account the effect of air bubbles in concrete (as a material manufacturing defect) on interfacial stresses, in reinforced concrete beams, strengthening with an externally bonded FRP composite plate. Both even distribution and uneven distribution of the air bubbles are taken into account and the effective properties of RC beams with air bubbles are defined by theoretical formula with an additional term of porosity. In particular, reliable evaluation of the adhesive shear stress and of the stress in the composite plates is mandatory in order to predict the beam's failure load. The model is based on equilibrium and deformations compatibility requirements in and all parts of the strengthened beam, i.e. the concrete beam, the FRP plate and the adhesive layer. Numerical results from the present analysis are presented both to demonstrate the advantages of the present solution over existing ones and to illustrate the main characteristics of interfacial stress distributions. This research is helpful for the understanding on mechanical behaviour of the interface and design of the hybrid structures.

**Keywords:** imperfect RC beam; air bubbles, interfacial stresses; strengthening; composite plates

## 1. Introduction

Among the new construction techniques, the rehabilitation of existing structures using composite materials is an effective solution to deal with certain natural phenomena. The purpose of this paper is the study of the phenomenon of separation of the composite plate, due to the high interface stresses at the edge of the plate bonded in a reinforced concrete beam strengthening with composite materials (Tounsi 2006). In recent years, several research studies have been carried out on the rehabilitation method (Abualnour *et al.* 2019, Hassaine Daouadji *et al.* 2016, 2019, Sharif *et al.* 2020, Antar *et al.* 2019, Benyoucef *et al.* 2007, Rabia *et al.* 2019, Bensattalah *et al.* 2016, 2018, Abdederak *et al.* 2018, Abdelhak *et al.* 2016, Belkacem *et al.* 2016, 2018, Daouadji and Adim 2016a, b, Hamrat *et al.* 2020, Hassaine Daouadji 2013, 2017, Hadj *et al.* 2019, Mahi *et al.* 2014, Guenaneche *et al.* 2014, Krour *et al.* 2014, Mohammadimehr *et al.* 2018, Panjehpour *et al.* 2014, Rabahi *et al.* 2019, Smith and Teng 2002, Tounsi 2006, Yeghnem *et al.* 2019, Bouakaz *et al.* 2014, Chedad *et al.* 2018, Chergui *et al.* 2019, Zidour *et al.* 2020, Benhenni *et al.* 2019a, Benferhat *et al.* 2016, Zine *et al.* 2020).

---

∗Corresponding author, Ph.D., Professor, E-mail: daouadjitahar@gmail.com; tahar.daouadji@univ-tiaret.dz

Interfacial stress studies accounting for the influence of adherend shear deformation are scarce. However, it is reasonable to assume that the shear stresses, which develop in the adhesive, are continuous across the adhesive-adherend interface. In addition, equilibrium requires the shear stress be zero at the free surface. The importance of including the shear-lag effect of the adherends was shown by several authors. The objective of the present investigation is to improve the method developed by Tounsi (2006) by assuming a parabolic shear stress across the depth of both FRP plate and RC beams and the effect air bubbles in the concrete. In view of this, it is desirable that a solution methodology be developed where the effect of adherend shear deformations can be included in a better manner so that the accuracy of Tounsi's solution can be properly assessed. Finally, the adopted improved model describes better the actual response of the hybrid beams and permits the evaluation of the adhesive stresses, the knowledge of which is very important in the design of such structures. It is believed that the present results will be of interest to civil and structural engineers and researchers (Benhenni *et al*. 2018, 2019a, Benferhat *et al*. 2018, Tayeb and Hassaine Daouadji 2020, Tahar *et al*. 2020, Rabia *et al*. 2016, Rabahi *et al*. 2016, 2020, Daouadji and Benferhat 2016).

In this article, we have shown the influence of the air bubbles (as a material manufacturing defect) of a reinforced concrete beam on the evolution of the composite-concrete interface stresses. An improved method for calculating interface stresses has been developed by Hassaine Daouadji *et al*. (2016). The anisotropic nature of the composite materials was taken into account in the theoretical analysis assuming a linear distribution of stresses across the thickness of the adhesive layer. We noticed through the results obtained that the maximum interface stresses calculated by the present method coincide perfectly with those from the literature.

## 2. Theoretical formulatio and solutions procedure

### 2.1 Material properties of the imperfect concrete beams

Due to the manufacturing defects of concrete such as the air bubbles "$\alpha$" which are the subject of the subject, the Young's modulus ($E_1$) of the imperfect reinforced concrete beam can be written as a function of the volume of the material. The mathematical form of porosity in concrete which can be presented in the form below

$$\bar{E}_1 = E_b(1 - \alpha) \tag{1}$$

$$\sigma_{ij} = (1 - \alpha)E_{ij}\varepsilon_{ij} \tag{2}$$

where $E_b$ is the elastic constants of concrete and "$\alpha$" is the index of air bubbles in concrete.

### 2.2 Assumptions of the present solution

The present analysis takes into consideration the transverse shear stress and strain in the beam and the plate but ignores the transverse normal stress in them. One of the analytical approach proposed by Hassaine Daouadji *et al*. (2016) for concrete beam strengthened with a bonded FRP Plate (Fig. 1) was used in order to compare it with analytical analysis. The analytical approach (Hassaine Daouadji *et al*. 2016) is based on the following assumptions:
  • Elastic stress strain relationship for concrete, composite and adhesive;
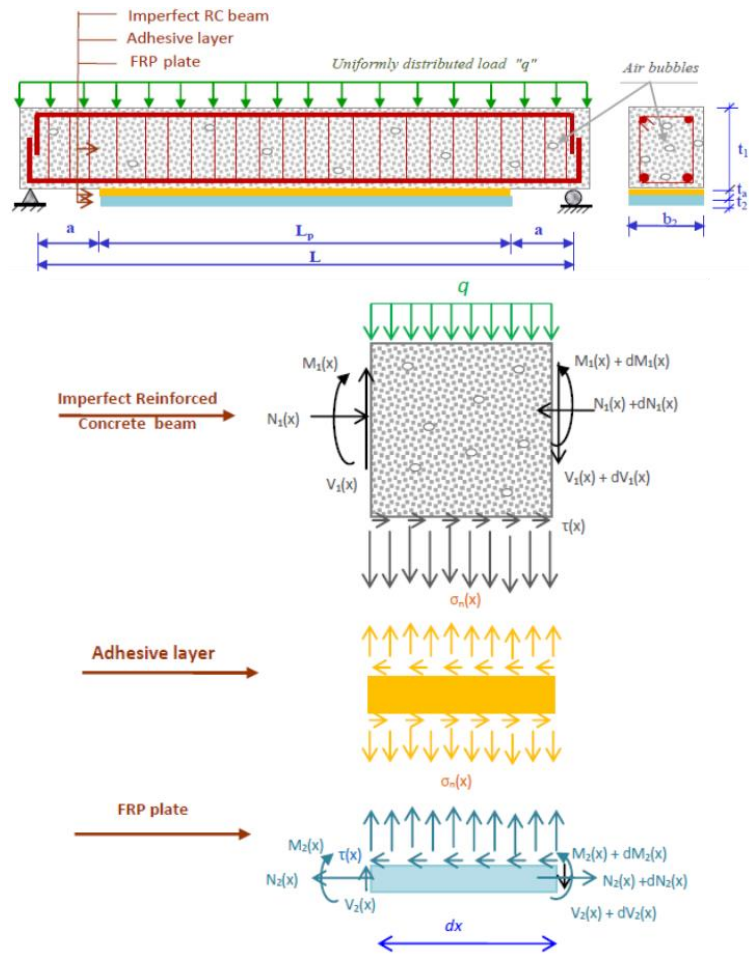  • There is a perfect bond between the composite plate and the RC beam;

Fig. 1 Simply supported imperfect RC beam strengthened with bonded FRP plate

• The adhesive is assumed to only play a role in transferring the stresses from the concrete to the composite plate reinforcement;

• The stresses in the adhesive layer do not change through the direction of the thickness.

Since the composite laminate is an orthotropic material, its material properties vary from layer to layer. In analytical study (Hassaine Daouadji *et al*. 2016), the laminate theory is used to determine the stress and strain behaviors of the externally bonded composite plate in order to investigate the whole mechanical performance of the composite-strengthened structure. The laminate theory is used to estimate the strain of the symmetrical composite plate. The Young's modulus ($E_1$) of the imperfect concrete beam can be written as a functions of thickness coordinate. Several forms of porosity (air bubbles in concrete) have been studied in the present work, such as "O", "V" and X".

Distribution forms of the air bubbles:

• Uniform distribution of the air bubbles

$$E_1 = E_b(1 - \alpha) \tag{3}$$

• Form "X" distribution shape of the air bubbles

$$E_1 = E_b - \alpha E_b (2\frac{z}{t_1}) \tag{4}$$

• Form "O" distribution shape of the air bubbles

$$E_1 = E_b - \alpha E_b (1 - 2\frac{|z|}{t_1}) \tag{5}$$

• Inverted form "V" distribution shape of the air bubbles

$$E_1 = E_b - \alpha E_b (\frac{1}{2} + \frac{z}{t_1}) \tag{6}$$

• Form "V" distribution shape of the air bubbles

$$E_1 = E_b - \alpha E_b (\frac{1}{2} - \frac{z}{t_1}) \tag{7}$$

On the other hand, the laminate theory is used to determine the stress and strain of the externally bonded composite plate in order to investigate the whole mechanical performance of the composite strengthened structure. The effective modules of the composite laminate are varied by the orientation of the fibre directions and arrangements of the laminate patterns. The classical laminate theory is used to estimate the strain of the composite plate, i.e.,

The fundamental equation of the laminate theory

$$\begin{Bmatrix} \varepsilon^0 \\ k \end{Bmatrix} = \begin{bmatrix} A' & B' \\ C' & D' \end{bmatrix} \begin{Bmatrix} N \\ M \end{Bmatrix} \tag{8}$$

$$
\begin{aligned}
[A'] &= [A]^{-1} + [A]^{-1}[B][D^*]^{-1}[B][A]^{-1} \\
[B'] &= -[A]^{-1}[B][D^*]^{-1} \\
[C'] &= [B']^T \\
[D'] &= [D^*]^{-1} \\
[D^*] &= [D] - [B][A]^{-1}[B]
\end{aligned} \tag{9}
$$

The terms of the matrices $[A]$, $[B]$ and $[D]$ are written as

[A]: Extensional matrix

$$A_{ij} = \sum_{k=1}^{NN} \bar{Q}_{ij}^k ((y_2)_k - (y_2)_{k-1}) \tag{10}$$

[B]: Extensional –bending coupled matrix

$$B_{ij} = \frac{1}{2} \sum_{k=1}^{NN} \bar{Q}_{ij}^k ((y_2^2)_k - (y_2^2)_{k-1}) \tag{11}$$

[D]: Flexural matrix

$$D_{ij} = \frac{1}{3} \sum_{k=1}^{NN} \bar{Q}_{ij}^k ((y_2^3)_k - (y_2^3)_{k-1}) \tag{12}$$

The subscript *NN* represents the number of laminate layers of the FRP plate, the transformed

stiffness matrix $[\bar{Q}_{ij}]$ varies with the orientation of the fibers of each layer, then $[\bar{Q}_{ij}]$ can be estimated by using the off-axis orthotropic plate theory, where

The transformed stiffness matrix $[\bar{Q}_{ij}]$

$$\overline{Q}_{ij} = \begin{bmatrix} \bar{Q}_{11} & \bar{Q}_{12} & 0 \\ \bar{Q}_{21} & \bar{Q}_{22} & 0 \\ 0 & 0 & \bar{Q}_{33} \end{bmatrix} \tag{13}$$

where $m = \cos(\theta_j)$ et $n = \sin(\theta_j)$

$$\overline{Q}_{11} = Q_{11}m^4 + 2(Q_{12} + 2Q_{33})m^2n^2 + Q_{22}n^4 \tag{14}$$

$$\overline{Q}_{12} = (Q_{11} + Q_{22} - 4Q_{33})m^2n^2 + Q_{12}(n^4 + m^4) \tag{15}$$

$$\overline{Q}_{22} = Q_{11}n^4 + 2(Q_{12} + 2Q_{33})m^2n^2 + Q_{22}m^4 \tag{16}$$

$$\overline{Q}_{33} = (Q_{11} + Q_{22} - 2Q_{12} - 2Q_{33})m^2n^2 + Q_{33}(n^4 + m^4) \tag{17}$$

and

$$Q_{11} = \frac{E_1}{1 - v_{12}v_{21}} \tag{18}$$

$$Q_{22} = \frac{E_2}{1 - v_{12}v_{21}} \tag{19}$$

$$Q_{12} = \frac{v_{12}E_2}{1 - v_{12}v_{21}} = \frac{v_{21}E_1}{1 - v_{12}v_{21}} \tag{20}$$

$$Q_{33} = G_{12} \tag{21}$$

where $j$ is number of the layer; $h$, $\bar{Q}_{ij}$ and $\theta_j$ are respectively the thickness, the Hooke's elastic tensor and the fibers orientation of each layer.

### 2.3 Shear stress distribution along the FRP - concrete interface

The governing differential equation for the interfacial shear stress is expressed as Hassaine Daouadji *et al.* (2016)

$$\frac{d^2\tau(x)}{dx^2} - \frac{\left(A'_{11} + \frac{b_2}{E_1A_1} + \frac{\left(y_1 + \frac{t_2}{2}\right)\left(y_1 + t_a + \frac{t_2}{2}\right)}{E_1I_1D'_{11} + b_2}b_2D'_{11}\right)}{\frac{1}{\frac{t_a}{G_a} + \frac{t_1}{4G_1}}}\tau(x) + \frac{\left(\frac{(y_1 + t_2/2)}{E_1I_1D'_{11} + b_2}D'_{11}\right)}{\frac{1}{\frac{t_a}{G_a} + \frac{t_1}{4G_1}}}V_T(x) = 0 \tag{22}$$

For simplicity, the general solutions presented below are limited to loading which is either concentrated or uniformly distributed over part or the whole span of the beam, or both. For such loading, $d^2V_T(x)/dx^2 = 0$, and the general solution to Eq. (6) is given by

$$\tau(x) = B_1 \cosh(\phi x) + B_2 \sinh(\phi x) + \frac{1}{\phi^2 \left(\frac{t_a}{G_a} + \frac{t_1}{4G_1}\right)} \left(\frac{y_1 + \frac{t_2}{2}}{E_1 I_1 D'_{11} + b_2} D'_{11}\right) V_T(x) \tag{23}$$

where

$$\phi = \left[\frac{\left(A'_{11} + \frac{b_2}{E_1 A_1} + \frac{(y_1 + t_2/2)(y_1 + t_a + t_2/2)}{E_1 I_1 D'_{11} + b_2} b_2 D'_{11}\right)}{\frac{1}{\frac{t_a}{G_a} + \frac{t_1}{4G_1}}}\right]^{\frac{1}{2}} \tag{24}$$

And $B_1$ and $B_2$ are constant coefficients determined from the boundary conditions. In the present study, a simply supported beam has been investigated which is subjected to a uniformly distributed load (Fig. 1). The interfacial shear stress for this uniformly distributed load at any point is written as (Hassaine Daouadji *et al*. 2016)

$$\tau(x) = \left[\frac{0.5.a y_1}{E_1 I_1 \left(\frac{t_a}{G_a} + \frac{t_1}{4G_1}\right)}(l - a) - \frac{1}{\left(\frac{t_a}{G_a} + \frac{t_1}{4G_1}\right)\phi^2}\left(\frac{y_1 + 0.5 t_2}{E_1 I_1 D'_{11} + b_2} D'_{11}\right)\right]\frac{q e^{-\lambda x}}{\phi}$$
$$+ \frac{1}{\phi^2 \left(\frac{t_a}{G_a} + \frac{t_1}{4G_1}\right)}\left(\frac{y_1 + 0.5 t_2}{E_1 I_1 D'_{11} + b_2} D'_{11}\right) q \left(\frac{l}{2} - a - x\right) \quad 0 \leq x \leq L_P \tag{25}$$

where $q$ is the uniformly distributed load and $x$; $a$; $L$ and $L_p$ are defined in Fig. 1.

### *2.4 Normal stress distribution along the FRP - concrete interface*

The following governing differential equation for the interfacial normal stress (Hassaine Daouadji *et al*. 2016).

$$\frac{d^4 \sigma_n(x)}{dx^4} + K_n \left(D'_{11} + \frac{b_2}{E_1 I_1}\right)\sigma_n(x) - K_n \left(D'_{11}\frac{t_2}{2} - \frac{y_1 b_2}{E_1 I_1}\right)\frac{d\tau(x)}{dx} + \frac{q K_n}{E_1 I_1} = 0 \tag{26}$$

The general solution to this fourth-order differential equation is

$$\sigma_n(x) = e^{-\beta x}[B_3 \cos(\eta x) + B_4 \sin(\eta x)] + e^{\beta x}[B_5 \cos(\eta x) + B_6 \sin(\eta x)]$$
$$- \zeta_1 \frac{d\tau(x)}{dx} - \frac{q}{D'_{11} E_1 I_1 + b_2} \tag{27}$$

For large values of $x$ it is assumed that the normal stress approaches zero and, as a result, $B_5 = B_6 = 0$. The general solution therefore becomes

$$\sigma_n(x) = e^{-\beta x}[B_3 \cos(\eta x) + B_4 \sin(\eta x)] - \zeta_1 \frac{d\tau(x)}{dx} - \frac{q}{D'_{11} E_1 I_1 + b_2} \tag{28}$$

where

$$\eta = \sqrt[4]{\frac{K_n}{4}\left(D'_{11} + \frac{b_2}{E_1 I_1}\right)} \tag{29}$$

$$\zeta_1 = \left( \frac{y_1 b_2 - D'_{11} E_1 I_1 t_2 / 2}{D'_{11} E_1 I_1 + b_2} \right) \tag{30}$$

As is described by Hassaine Daouadji *et al*. (2016), the constants $B_3$ and $B_4$ in Eq. (28) are determined using the appropriate boundary conditions and they are written as follows

$$B_3 = \frac{K_n}{2\eta^3 E_1 I_1} [V_T(0) + \eta M_T(0)] - \frac{\zeta_2}{2\eta^3} \tau(0) + \frac{\zeta_1}{2\eta^3} \left( \frac{d^4 \tau(0)}{dx^4} + \eta \frac{d^3 \tau(0)}{dx^3} \right) \tag{31}$$

$$B_4 = -\frac{K_n}{2\eta^2 E_1 I_1} M_T(0) - \frac{\zeta_1}{2\eta^2} \frac{d^3 \tau(0)}{dx^3} \tag{32}$$

$$\zeta_2 = b_2 K_n \left( \frac{y_1}{E_1 I_1} - \frac{D'_{11} t_2}{2 b_2} \right) \tag{33}$$

The above expressions for the constants $B_3$ and $B_4$ has been left in terms of the bending moment $M_T(0)$ and shear force $V_T(0)$ at the end of the soffit plate. With the constants $B_3$ and $B_4$ determined, the interfacial normal stress can then be found using Eq. (28).

## 3. Results: Discussion and analysis

In this section, numerical results are presented for the prediction of the normal and shear stresses of RC beams contains air bubbles strengthening with an externally bonded FRP composite plate and subjected to uniformly distributed load. To verify the accuracy of the present solution, the obtained results are compared with some existing results in the literature. Numerical and graphical results are presented to show the effect of the volume fraction of air bubbles in the interfacial stresses of RC beam strengthened with FRP plate. The geometry and materials properties used in this study are summarized in the Table 1.

At first, a comparison study is presented in Table 2 between the results of the present study and those given by Tounsi (2008) for the case of perfect ($\alpha = 0$) and imperfect ($\alpha \neq 0$) RC beams strengthened with CFRP, GFRP and Steel plates, respectively. The beams are considered subjected to a uniformly distributed load. The thickness of FRP plate is taken to be $t_2 = 4$ mm. The comparisons show that the interface stress predicted by the present study are in good agreement with those of Tounsi (2008) for perfect RC beams ($\alpha = 0$) and takes greater values when the beams contains the air bubbles.

Table 1 Dimensions and material properties

| Component | $E$ (GPa) | $G$ (GPa) | Width (mm) | Depth (mm) | Length (mm) |
|---|---|---|---|---|---|
| RC beam | 30 | / | $b_1 = 200$ | $t_1 = 300$ | 2800 |
| CFRP plate | 140 | 5 | $b_2 = 200$ | $t_2 = 4$ | 2400 |
| GFRP plate | 50 | 5 | $b_2 = 200$ | $t_2 = 4$ | 2400 |
| Steel plate | 200 | / | $b_2 = 200$ | $t_2 = 4$ | 2400 |
| Adhésif | 3 | / | $b_2 = 200$ | $t_a = 2$ | 2400 |

Table 2 Effect of air bubbles on the interface stress of a RC beam strengthened by CFRP, GFRP and steel plates for uniformly distributed loading ($t_2 = 4$)

| Theory | % air bubbles in the concrete | GFRP | | CFRP | | Steel | |
|---|---|---|---|---|---|---|---|
| | | $\tau(x)$ | $\sigma_n(x)$ | $\tau(x)$ | $\sigma_n(x)$ | $\tau(x)$ | $\sigma_n(x)$ |
| Tounsi (2008) | $\alpha = 0$ | 1.0885 | 0.826 | 1.791 | 1.078 | 2.120 | 1.175 |
| Present RC beam | $\alpha = 0$ | 1.0885 | 0.826 | 1.794 | 1.078 | 2.120 | 1.175 |
| | $\alpha = 0.02$ | 1.0989 | 0.83679 | 1.8114 | 1.0907 | 2.1420 | 1.1880 |
| | $\alpha = 0.04$ | 1.1125 | 0.84774 | 1.8316 | 1.1037 | 2.1643 | 1.2012 |
| | $\alpha = 0.06$ | 1.1264 | 0.85897 | 1.8526 | 1.1173 | 2.1867 | 1.2147 |

Table 3 Air bubbles effect and the thickness ratio $t_1/b_1$ on the interface stresses for a RC beam strengthened by CFRP, GFRP and steel plates for uniformly distributed loading ($t_2 = 6$)

| $t_1/b_1$ | % air bubbles in the concrete | GFRP | | CFRP | | Steel | |
|---|---|---|---|---|---|---|---|
| | | $\tau(x)$ | $\sigma_n(x)$ | $\tau(x)$ | $\sigma_n(x)$ | $\tau(x)$ | $\sigma_n(x)$ |
| 1 | $\alpha = 0$ | 3.2875 | 2.8018 | 5.0305 | 3.4377 | 5.7974 | 3.6640 |
| | $\alpha = 0.04$ | 3.3669 | 2.8751 | 5.1304 | 3.5142 | 5.8965 | 3.7366 |
| | $\alpha = 0.06$ | 3.4084 | 2.9134 | 5.1820 | 3.5536 | 5.9475 | 3.7741 |
| 1.5 | $\alpha = 0$ | 1.3224 | 1.1228 | 2.1287 | 1.4362 | 2.4948 | 1.5530 |
| | $\alpha = 0.04$ | 1.3545 | 1.1519 | 2.1734 | 1.4689 | 2.5412 | 1.5850 |
| | $\alpha = 0.06$ | 1.3712 | 1.1672 | 2.1965 | 1.4859 | 2.5654 | 1.6017 |
| 2 | $\alpha = 0$ | 0.68437 | 0.58051 | 1.1365 | 0.76249 | 1.3472 | 0.83270 |
| | $\alpha = 0.04$ | 0.70105 | 0.59553 | 1.1613 | 0.78034 | 1.3740 | 0.85071 |
| | $\alpha = 0.06$ | 0.70973 | 0.60340 | 1.1740 | 0.78958 | 1.3877 | 0.85993 |

Table 4 Air bubbles effect and the thickness ratio $t_2/b_2$ on the interface stresses for a RC beam strengthened by CFRP, GFRP and steel plates for uniformly distributed loading

| $t_2/b_2$ | % air bubbles in the concrete | GFRP | | CFRP | | Steel | |
|---|---|---|---|---|---|---|---|
| | | $\tau(x)$ | $\sigma_n(x)$ | $\tau(x)$ | $\sigma_n(x)$ | $\tau(x)$ | $\sigma_n(x)$ |
| 0.02 | $\alpha = 0$ | 1.0856 | 0.82607 | 1.7914 | 1.0779 | 2.1204 | 1.1751 |
| | $\alpha = 0.04$ | 1.1125 | 0.84774 | 1.8316 | 1.1037 | 2.1643 | 1.2012 |
| | $\alpha = 0.06$ | 1.1264 | 0.85897 | 1.8526 | 1.1173 | 2.1867 | 1.2147 |
| 0.03 | $\alpha = 0$ | 1.3224 | 1.1228 | 2.1287 | 1.4362 | 2.4948 | 1.5530 |
| | $\alpha = 0.04$ | 1.3545 | 1.1519 | 2.1734 | 1.4689 | 2.5412 | 1.5850 |
| | $\alpha = 0.06$ | 1.3712 | 1.1672 | 2.1965 | 1.4859 | 2.5654 | 1.6017 |
| 0.04 | $\alpha = 0$ | 1.5128 | 1.3915 | 2.3774 | 1.7466 | 2.7637 | 1.8756 |
| | $\alpha = 0.04$ | 1.5488 | 1.4274 | 2.4243 | 1.7848 | 2.8106 | 1.9122 |
| | $\alpha = 0.06$ | 1.5675 | 1.4460 | 2.4484 | 1.8046 | 2.8349 | 1.9314 |

Tables 3 and 4 aim to analyze the effect of the volume fraction of the air bubbles versus the thickness ratio $t_1/b_1$ and $t_2/b_2$ on the interface stresses for a RC beam strengthened by CFRP, GFRP

Table 5 Effect of the air bubbles distribution shape on the interface stresses of a RC beam strengthened by CFRP, GFRP and steel plates for uniformly distributed loading

| FRP plate | Distribution shape of the porosity | % air bubbles in the concrete | | | | | |
|---|---|---|---|---|---|---|---|
| | | $\alpha = 0.02$ | | $\alpha = 0.04$ | | $\alpha = 0.06$ | |
| | | $\tau(x)$ | $\sigma_n(x)$ | $\tau(x)$ | $\sigma_n(x)$ | $\tau(x)$ | $\sigma_n(x)$ |
| GFRP | Uniform distribution shape | 1.0989 | 0.83679 | 1.1125 | 0.84774 | 1.1264 | 0.85897 |
| | Form "O" distribution shape | 1.0906 | 0.83012 | 1.0958 | 0.83423 | 1.1009 | 0.83841 |
| | Form "X" distribution shape | 1.0938 | 0.83268 | 1.1021 | 0.83935 | 1.1105 | 0.84618 |
| | Form "V" distribution shape | 1.0963 | 0.83471 | 1.1072 | 0.84353 | 1.1184 | 0.85259 |
| | Inverted form "V" distribution shape | 1.0882 | 0.82814 | 1.0906 | 0.83012 | 1.0932 | 0.83216 |
| CFRP | Uniform distribution shape | 1.8114 | 1.0907 | 1.8316 | 1.1037 | 1.8526 | 1.1173 |
| | Form "O" distribution shape | 1.7990 | 1.0829 | 1.8066 | 1.0878 | 1.8143 | 1.0927 |
| | Form "X" distribution shape | 1.8036 | 1.0858 | 1.8162 | 1.0939 | 1.8288 | 1.1020 |
| | Form "V" distribution shape | 1.8074 | 1.0882 | 1.8239 | 1.0988 | 1.8407 | 1.1095 |
| | Inverted form "V" distribution shape | 1.7952 | 1.0805 | 1.7990 | 1.0829 | 1.8028 | 1.0853 |
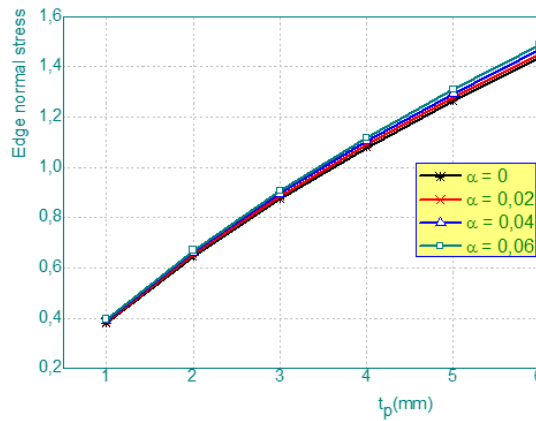


Fig. 2 Effect of CFRP thickness on normal stress for different volume fraction of the air bubbles
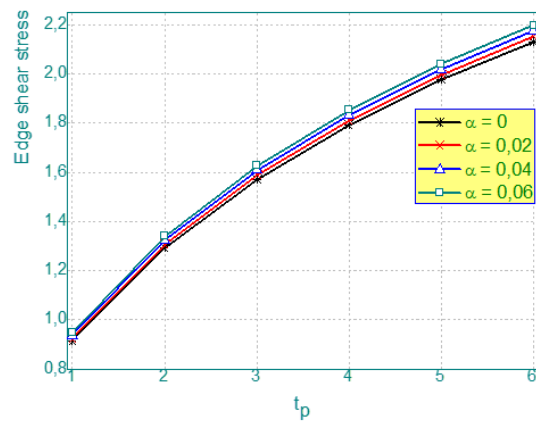


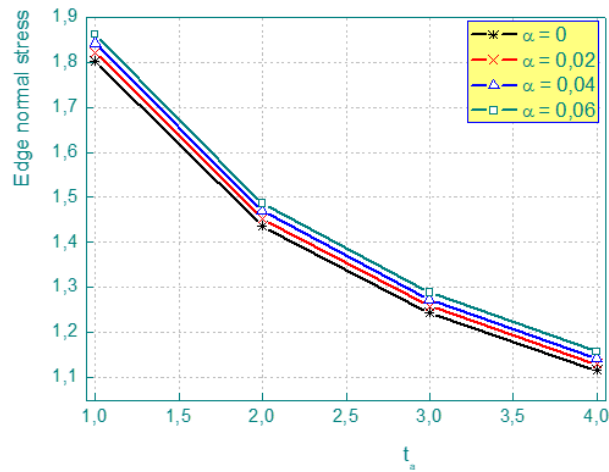Fig. 3 Effect of CFRP thickness on shear stress for different volume fraction of the air bubbles

Fig. 4 Effect of the thickness of the adhesive layer on the normal stress for different values of volume fraction of air bubbles
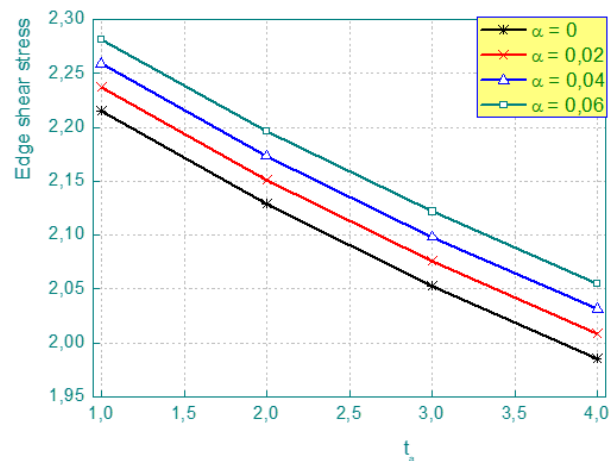


Fig. 5 Effect of the thickness of the adhesive layer on the shear stress for different values of volume fraction of air bubbles

and steel plates and subjected to uniformly distributed load, respectively. The thickness of FRP plate is taken to be ($t_2 = 6$ mm) in Table 3. It is observed that as the volume fraction of the air bubbles and the thickness ratio $t_1/b_1$ increase, the interfacial shear and normal stresses increase. This last diminishes with the increase of the thickness ratio $t_1/b_1$.

The effect of the distribution shape of the air bubbles on the interface stresses of a RC beam strengthened by CFRP, GFRP and steel plates subjected to a uniformly distributed load is presented in Table 5 for different values of the volume fraction of the air bubbles ($\alpha = 0$, $\alpha = 0.04$ and $\alpha = 0.06$). It can be seen that the interfacial stresses slightly decrease for the uneven distribution shape of the air bubbles in the RC beam and takes maximum values for the even distribution shape.

Figs. 2 and 3 show the effect of CFRP thickness on normal and shear stresses a RC beam strengthened by CFRP plate versus the thickness of FRP (tp) plate for different volume fraction of
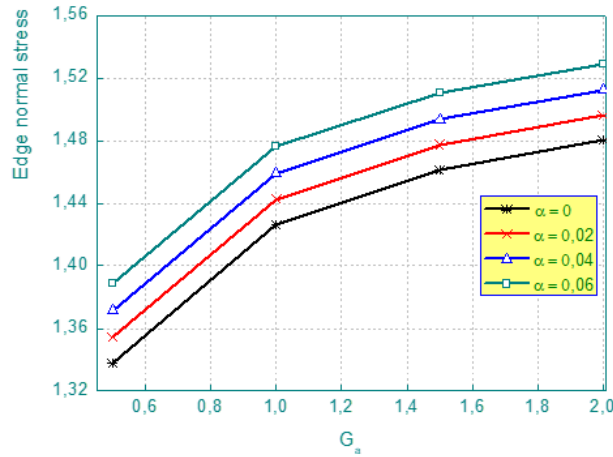
Fig. 6 Effect of shear modulus of the adhesive on the normal stress for different volume fraction of the air bubbles
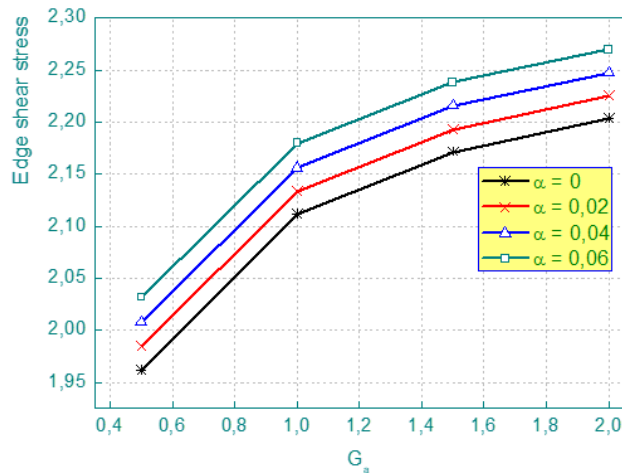


Fig. 7 Effect of shear modulus of the adhesive on the shear stress for different volume fraction of the air bubbles

the air bubbles. it can be noted that the effect of the volume fraction of the air bubbles becomes greater on the interface stresses when the thickness of the reinforcement plate increases. The figures show that the RC beam with air bubbles undergo greater interfacial stresses.

The effect of the thickness of the adhesive layer on the normal and the shear stresses of a RC beam strengthened by CFRP plate for different values of volume fraction of air bubbles is presented in Figs. 4 and 5, respectively. It can be seen that increasing the thickness of the adhesive layer leads to a significant reduction in the interfacial stresses.

Figs. 6 and 7 show the effect of shear modulus of the adhesive on the normal and shear stresses for different volume fraction of the air bubbles of a RC beam strengthened by CFRP plate and subjected to a uniformly distributed load. It can be seen that the increase in the shear modulus of the adhesive and the volume fraction of the air bubbles yields an increase in the interfacial stresses.

## 4. Conclusions

The prediction of the interfacial stresses in RC beams contains the air bubbles and strengthening with an externally bonded FRP composite plate have been presented based on the analytical method. Both even distribution and uneven distribution of the air bubbles are taken into account in this study. Effective properties of RC beams with air bubbles are defined by theoretical formula with an additional term of porosity. Numerical comparison between the existing solutions and the present new solution has been carried out for perfect RC beams. The results reveal that RC beams contains air bubbles undergo greater the normal and shear stresses. The results also reveal that the interfacial stresses decrease for the uneven distribution shape of the air bubbles in the RC beam and takes maximum values for the even distribution shape.

## Acknowledgments

## References

Abdederak, R., Hassaine Daouadji, T., Benferhat, R. and Adim, B. (2018), "Nonlinear analysis of damaged RC beams strengthened with glass fiber reinforced polymer plate under symmetric loads", *Earthq. Struct.*, **15**(2), 113-122. https://doi.org/10.12989/eas.2018.15.2.113.

Abdelhak, Z., Hadji, L., Khelifa, Z., Hassaine Daouadji, T. and Adda Bedia, E.A. (2016), "Analysis of buckling response of functionally graded sandwich plates using a refined shear deformation theory", *Wind Struct.*, **22**(3), 291-305. https://doi.org/10.12989/was.2016.22.3.291.

Abualnour, M., Chikh, A., Hebali, H., Kaci, A. and Tounsi, A. (2019), "Thermomechanical analysis of antisymmetric laminated reinforced composite plates using a new four variable trigonometric refined plate theory", *Comput. Concrete*, **24**(6), 489-498. http://dx.doi.org/10.12989/cac.2019.24.6.489.

Antar, K., Amara, K., Benyoucef, S., Bouazza, M. and Ellali, M. (2019), "Hygrothermal effects on the behavior of reinforced-concrete beams strengthened by bonded composite laminate plates", *Struct. Eng. Mech.*, **69**(3), 327-334. https://doi.org/10.12989/sem.2019.69.3.327.

Belkacem, A. and Hassaine Daouadji, T. (2016), "Effects of thickness stretching in FGM plates using a quasi-3D higher order shear deformation theory", *Adv. Mater. Res.*, **5**(4), 223-244. https://doi.org/10.12989/amr.2016.5.4.223.

Belkacem, A., Tahar, H.D., Abderrezak, R., Amine, B.M., Mohamed, Z. and Boussad, A. (2018), "Mechanical buckling analysis of hybrid laminated composite plates under different boundary conditions", *Struct. Eng. Mech.*, **66**(6), 761-769. https://doi.org/10.12989/sem.2018.66.6.761.

Benferhat, R., Hassaine Daouadji, T., Said Mansour, M. and Hadji, L. (2016), "Effect of porosity on the bending and free vibration response of functionally graded plates resting on Winkler-Pasternak foundations", *Earthq. Struct.*, **10**(6), 1429-1449. https://doi.org/10.12989/eas.2016.10.6.1429.

Benferhat, R., Rabahi, A., Hassaine Daouadji, T., Boussad, A. and Adim, B. (2018), "Analytical analysis of the interfacial shear stress in RC beams strengthened with prestressed exponentially-varying properties plate", *Adv. Mater. Res.*, **7**(1), 29-44. https://doi.org/10.12989/amr.2018.7.1.029.

Benhenni, M.A., Daouadji, T.H., Abbes, B., Adim, B., Li, Y. and Abbes, F. (2018), "Dynamic analysis for anti-symmetric cross-ply and angle-ply laminates for simply supported thick hybrid rectangular plates",

*Adv. Mater. Res.*, **7**(2), 83-103. https://doi.org/10.12989/amr.2018.7.2.119.

Benhenni, M.A., Hassaine Daouadji, T., Abbes, B., Abbes, F., Li, Y. and Adim, B. (2019a), "Numerical analysis for free vibration of hybrid laminated composite plates for different boundary conditions", *Struct. Eng. Mech.*, **70**(5), 535-549. https://doi.org/10.12989/sem.2019.70.5.535.

Benhenni, M.A., Adim, B., Daouadji, T.H., Abbès, B., Abbès, F., Li, Y. and Bouzidane, A. (2019b), "A comparison of closed form and finite element solutions for the free vibration of hybrid cross ply laminated plates", *Mech. Compos. Mater.*, **55**(2), 181-194. https://doi.org/10.1007/s11029-019-09803-2.

Bensattalah, T., Hassaine Daouadji, T., Zidour, M., Tounsi, A. and Adda Bedia, E.A. (2016), "Investigation of thermal and chirality effects on vibration of single walled carbon nanotubes embedded in a polymeric matrix using nonlocal elasticity theories", *Mech. Compos. Mater.*, **52**(4), 555-568. https://doi.org/10.1007/s11029-016-9606-z.

Bensattalah, T., Zidour, M. and Hassaine Daouadji, T. (2018), "Analytical analysis for the forced vibration of CNT surrounding elastic medium including thermal effect using nonlocal Euler-Bernoulli theory", *Adv. Mater. Res.*, **7**(3), 163-174. https://doi.org/10.12989/amr.2018.7.3.163.

Benyoucef, S, Tounsi, A., Meftah, S.A. and Adda Bedia, E.A. (2007), "Approximate analysis of the interfacial stress concentrations in FRP-RC hybrid beams", *Compos. Interf.*, **13**(7), 561-571. https://doi.org/10.1163/156855406778440758.

Bouakaz, K., Hassaine Daouadji, T., Meftah, S.A. and Ameur, M. (2014), "A numerical analysis of steel beams strengthened with composite materials", *Mech. Compos. Mater.*, **50**(4), 685-696. https://doi.org/10.1007/s11029-014-9435-x.

Chedad, A., Daouadji, T.H., Abderezak, R., Adim, B., Abbes, B., Rabia, B. and Abbes, F. (2018), "A high-order closed-form solution for interfacial stresses in externally sandwich FGM plated RC beams", *Adv. Mater. Res.*, **6**(4), 317-328. https://doi.org/10.12989/amr.2017.6.4.317.

Chergui, S., Hassaine Daouadji, T., Mostefa, H., Bougara, A., Abbes, B. and Amziane, S. (2019), "Interfacial stresses in damaged RC beams strengthened by externally bonded prestressed GFRP laminate plate: Analytical and numerical study", *Adv. Mater. Res.*, 8(3), 197-217. https://doi.org/10.12989/amr.2019.8.3.197.

Daouadji, T.H. and Adim, B. (2016a), "An analytical approach for buckling of functionally graded plates", *Adv. Mater. Res.*, **5**(3), 141-169. https://doi.org/10.12989/amr.2016.5.3.141.

Daouadji, T.H. and Adim, B. (2016b), "Theoretical analysis of composite beams under uniformly distributed load", *Adv. Mater. Res.*, **5**(1), 1-9. https://doi.org/10.12989/amr.2016.5.1.001.

Daouadji, T.H. and Benferhat, R. (2016), "Bending analysis of an imperfect FGM plates under hygro-thermo-mechanical loading with analytical validation", *Adv. Mater. Res.*, **5**(1), 35-53. https://doi.org/10.12989/amr.2016.5.1.035.

Guenaneche, B., Tounsi, A. and Adda Bedia, E.A. (2014), "Effect of shear deformation on interfacial stress analysis in plated beams under arbitrary loading", *Adhes. Adhes.*, **48**, 1-13. https://doi.org/10.1016/j.ijadhadh.2013.09.016.

Hadj, B., Rabia, B. and Daouadji, T.H. (2019), "Influence of the distribution shape of porosity on the bending FGM new plate model resting on elastic foundations", *Struct. Eng. Mech.*, **72**(1), 823-832. https://doi.org/10.12989/sem.2019.72.1.061.

Hamrat, M., Bouziadi, F., Boulekbache, B., Daouadji, T.H., Chergui, S., Labed, A. and Amziane, S. (2020), "Experimental and numerical investigation on the deflection behavior of pre-cracked and repaired reinforced concrete beams with fiber-reinforced polymer", *Constr. Build. Mater.*, **249**, 118745. https://doi.org/10.1016/j.conbuildmat.2020.118745.

Hassaine Daouadji, T. (2013), "Analytical analysis of the interfacial stress in damaged reinforced concrete beams strengthened by bonded composite plates", *Strength Mater.*, **45**(5), 587-597. htttps://doi.org/10.1007/s11223-013-9496-4.

Hassaine Daouadji, T. (2017) "Analytical and numerical modeling of interfacial stresses in beams bonded with a thin plate", *Adv. Comput. Des.*, **2**(1), 57-69. https://doi.org/10.12989/acd.2017.2.1.057.

Hassaine Daouadji, T., Rabahi, A., Abbes, B. and Adim, B. (2016), "Theoretical and finite element studies of

interfacial stresses in reinforced concrete beams strengthened by externally FRP laminates plate", *J. Adhes. Sci. Technol.*, 30(12), 1253-1280. https://doi.org/10.1080/01694243.2016.1140703.

Hassaine Daouadji, T., Rabahi, A., Benferhat, R. and Adim, B. (2019), "Flexural behaviour of steel beams reinforced by carbon fibre reinforced polymer: Experimental and numerical study", *Struct. Eng. Mech.*, **72**(4), 409-419. https://doi.org/10.12989/sem.2019.72.4.409.

Krour, B., Bernard, F. and Tounsi, A. (2014), "Fibers orientation optimization for concrete beam strengthened with a CFRP bonded plate: A coupled analytical-numerical investigation", *Eng. Struct.*, **9**, 218-227. https://doi.org/10.1016/j.engstruct.2013.05.008.

Mahi, B.E., Benrahou, K.H., Belakhdar, K., Tounsi, A. and Bedia, E.A. (2014), "Effect of the tapered end of a FRP plate on the interfacial stresses in a strengthened beam used in civil engineering applications", *Mech. Compos. Mater.*, 50(4), 465-474. https://doi.org/10.1007/s11029-014-9433-z.

Mohammadimehr, M., Mehrabi, M. and Hadizadeh, H. (2018), "Surf ace and size dependent effects on static, buckling, and vibration of micro composite beam under thermomagnetic fields based on strain gradient theory", *Steel Compos. Struct.*, **26**(4), 513-531. https://doi.org/10.12989/scs.2018.26.4.513.

Panjehpour, M., Ali, A.A.A., Voo, Y.L. and Aznieta, F.N. (2014), "Effective compressive strength of strut in CFRP-strengthened reinforced concrete deep beams following ACI 318-11", *Comput. Concrete*, **13**(1), 135-165. https://doi.org/10.12989/cac.2014.13.1.135.

Rabahi, A., Hassaine Daouadji, T. Abbes, B. and Adim, B. (2016), "Analytical and numerical solution of the interfacial stress in reinforced-concrete beams reinforced with bonded prestressed composite plate", *J. Reinf. Plast. Compos.*, **35**(3) 258-272. https://doi.org/10.1177/0731684415613633.

Rabahi, A., Benferhat, R. and Hassaine Daouadji, T. (2019), "Elastic analysis of interfacial stresses in prestressed PFGM-RC hybrid beams", *Adv. Mater. Res.*, **7**(2), 83-103. https://doi.org/10.12989/amr.2018.7.2.083.

Rabahi, A., Hassaine Daouadji T. and Benferhat, R. (2020), "Analysis of interfacial stresses of the reinforced concrete foundation beams repairing with composite materials plate", *Coupled Syst. Mech.*, **9**(5), 473-498. http://dx.doi.org/10.12989/csm.2020.9.5.473.

Rabia, B., Hassaine Daouadji, T., Hadji, L. and Mansour, M. (2016), "Static analysis of the FGM plate with porosities", *Steel Compos. Struct.*, **21**(1), 123-136. https://doi.org/10.12989/scs.2016.21.1.123.

Rabia, B., Daouadji, T.H. and Abderezak, R. (2019), "Effect of distribution shape of the porosity on the interfacial stresses of the FGM beam strengthened with FRP plate", *Earthq. Struct.*, **16**(5), 601-609. https://doi.org/10.12989/eas.2019.16.5.601.

Sharif, A.M., Assi, N.A. and Al-Osta, M.A. (2020), "Use of UHPC slab for continuous composite steel-concrete girders", *Steel Compos. Struct.*, **34**(3), 321-332. https://doi.org/10.12989/scs.2020.34.3.321.

Smith, S.T. and Teng, J.G. (2002), "Interfacial stresses in plated beams", *Eng. Struct.*, **23**(7), 857-871. http://dx.doi.org/10.1016/S0141-0296(00)00090-0.

Tahar, H.D., Abderezak, R. and Rabia, B. (2020), "Flexural performance of wooden beams strengthened by composite plate", *Struct. Monit. Maint.*, **7**(3), 233-259. http://dx.doi.org/10.12989/smm.2020.7.3.233.

Tayeb, B. and Hassaine Daouadji, T. (2020), "Improved analytical solution for slip and interfacial stress in composite steel-concrete beam bonded with an adhesive", *Adv. Mater. Res.*, **9**(2), 133-153. https://doi.org/10.12989/amr.2020.9.2.133.

Tounsi, A. (2006), "Improved theoretical solution for interfacial stresses in concrete beams strengthened with FRP plate", *Int. J. Solids Struct.*, **43**(14-15), 4154-4174. https://doi.org/10.1016/j.ijsolstr.2005.03.074.

Tounsi, A., Hassaine Daouadji, T., Benyoucef, S. and Adda Bedia, E.A. (2008), "Interfacial stresses in FRP-plated RC beams: Effect of adherend shear deformations", *Int. J. Adhes. Adhes.*, **29**, 313-351. https://doi.org/10.1016/j.ijadhadh.2008.06.008.

Yeghnem, R., Sara, C., Kaci, A. and Tounsi, A. (2019), "A new higher-order shear and normal deformation theory for the buckling analysis of new type of FGM sandwich plates", *Struct. Eng. Mech.*, **72**(5), 653-673. https://doi.org/10.12989/sem.2019.72.5.653.

Zidour, M., Si Tayeb, T., Bensattalah, T., Heireche, H., Benahmed A. and Adda Bedia, E.A. (2020), "Mechanical buckling of FG-CNTs reinforced composite plate with parabolic distribution using Hamilton's energy principle", *Adv. Nano Res.*, **8**(2), 135-148. https://doi.org/10.12989/anr.2020.8.2.135.

Zine, A., Bourada, F., Benrahou, K.H., Adda Bedia, E.A., Mahmoud, S.R. and Tounsi, A. (2020), "Bending analysis of functionally graded porous plates via a refined shear deformation theory", *Comput. Concrete*, **26**(1), 63-74. http://dx.doi.org/10.12989/cac.2020.26.1.063.

*CC*